REPORT DOCUMENTATION PAGE

Form Approved OMB No. 0704-0188

1. AGENCY USE ONLY (*Leave Blank*)	2. REPORT DATE	3. REPORT TYPE AND DATES COVERED
	March 21, 1996	Final, Oct. 1995 to Feb. 1996

4. TITLE AND SUBTITLE

Melt Drawing/Coating of Oxide Fibers for Composite Materials Applications

5. FUNDING NUMBERS

F49620-95-C-0067

6. AUTHOR(S)

J.K.R. Weber, J.J. Felten, P.C. Nordine
W.M. Kriven

7. PERFORMING ORGANIZATION NAME(S) AND ADDRESS(ES)

Containerless Research, Inc.
910 University Place
Evanston, IL 60201-3149

8. PERFORMING ORGANIZATION REPORT NUMBER

AFPH1.0196

9. SPONSORING/MONITORING AGENCY NAME(S) AND ADDRESS(ES)

Dr. Alexander Pechenik
AFOSR/NA
Directorate of Aerospace and Materials Sciences
110 Duncan Ave., Bolling AFB, DC 20332-0001

10. SPONSORING/MONITORING AGENCY REPORT NUMBER

11. SUPPLEMENTARY NOTES

12a. DISTRIBUTION/AVAILABILITY STATEMENT

Approved for public release, distribution unlimited.

12b. DISTRIBUTION CODE

13. ABSTRACT (*Maximum 200 words*)

Undercooled oxide melts achieved a melt viscosity sufficient to draw mullite fibers whose chemical, microstructural, and mechanical properties were measured. Tensile strengths were 5.61 $\pm$ 0.71 GPa (810 $\pm$ 100 KSI) for as-drawn, amorphous fibers of 10-40 μm diameter and up to 1.0 GPa after crystallization by annealing in air. Melt drawing of YAG fibers was also demonstrated. Fiber coatings were formed by pulsed excimer laser ablation. Push-out tests on coated fibers imbedded in a ceramic matrix gave small values of the debonding shear strength, $\tau_d \approx 25$ MPa, for fibers coated with 2 $MgO{\cdot}SiO_2$ (enstatite), which provided an interphase-weakening effect. Somewhat larger values of τ_d were obtained for $LaPO_4$ coated fibers which provide an interface-weakening effect. Mullite fibers with YPO_4 coatings exhibited chemical and dimensional stability during a 2 hour anneal in an aluminum oxide matrix at 1500°C. The fiber-pulling process has potential for scale-up to produce high quality oxide fibers at less than $100 per pound.

14. SUBJECT TERMS

Fibers, Mullite, High Temperature, Ceramic Matrix Composite

15. NUMBER OF PAGES

38

16. PRICE CODE

17. SECURITY CLASSIFICATION OF REPORT	18. SECURITY CLASSIFICATION OF THIS PAGE	19. SECURITY CLASSIFICATION OF ABSTRACT	20. LIMITATION OF ABSTRACT
Unclassified	Unclassified	Unclassified	

FINAL TECHNICAL REPORT

Phase I SBIR

MELT DRAWING/COATING OF OXIDE FIBERS FOR COMPOSITE MATERIALS APPLICATIONS

Contract F49620-95-C-0067

Reporting Period
September, 1995 to February, 1996

for

AFOSR/PKA
110 Duncan Ave. Suite B115
Bolling AFB DC 20332-0001

by

Containerless Research, Inc.
910 University Place
Evanston, IL 60201-3149
847/467-2678

March 21, 1996

Table of Contents

List of Figures

Page

List of Tables

EXECUTIVE SUMMARY

Fibers cannot be drawn from the melts of many technologically interesting oxide materials. The reason is that the melts are too inviscid at temperatures above the melting point. Prior research at CRI and elsewhere has demonstrated that deep undercooling of oxide melts can be readily achieved under containerless conditions. Since the viscosity of molten oxides increases as the liquid cools, we theorized that fibers could be pulled from undercooled oxide melts. In Phase I, we proposed to (i) demonstrate the ability to pull fibers from undercooled melts; (ii) characterize the fibers in terms of mechanical and chemical properties and microstructures; (iii) investigate the deposition, properties, and performance in composites of interface-weakening coatings applied to the fibers; and (iv) determine the viability and cost of scaled-up fiber production. We focussed on the mullite composition of the alumino-silicate system.

The project objectives were met. Mullite fibers of high and reproducible purity and strength were obtained. The as-pulled fibers were amorphous with diameters ranging from 10-50 μm (fiber diameter decreased with pulling rate). They had room temperature tensile strengths equal to 5.61 $\pm$ 0.71 GPa or 810 $\pm$ 100 KSI.

The amorphous fibers were crystallized by heating to 1100-1500°C in air. Tensile strengths measured on three fibers that were crystallized at 1100-1200°C were 0.66, 0.78, and 1.0 GPa, comparable to values of $<$ 2 GPa reported for commercially available oxide fibers heated to the same temperature range. A considerable increase in high-temperature strength of the mullite fibers may be achieved by (i) adapting the process to pull continuous, long, and uniform diameter amorphous fibers and (ii) optimizing the conditions for crystallization of the amorphous fibers.

The ability to pull YAG fibers was also demonstrated in a few preliminary experiments. The YAG fibers were not characterized. The fiber pulling process can be applied to many other oxide systems. Several oxide melts have already been demonstrated to provide a sufficient viscosity when undercooled that fiber drawing would be possible.

Fiber coating and composite materials research was performed to investigate (i) lanthanum phosphate (monazite) coatings on YAG fibers in an aluminum oxide matrix, (ii) a five-layer, chemically stable system to form enstatite ($MgSiO_3$) coatings on sapphire in an alumina matrix, and (iii) yttrium phosphate coatings on the mullite fibers in a mullite matrix. Fiber push-out tests were performed to determine interphase or interface weakening effects of the coatings on the larger sapphire and YAG fibers, but were not possible on the smaller diameter mullite fibers. The YPO_4-coated mullite fibers in a mullite matrix were examined by SEM-EDS after the composite was heated to 1500°C for two hours. The coated fiber and matrix were chemically and dimensionally stable during the heating to 1500°C.

Fiber pulling rates were up to 30 cm/s in transient experiments that allowed fiber lengths up to 15 cm. The fiber diameters varied with the pulling rate. Much larger pulling rates and exceptionally uniform fiber diameters will be obtainable by modifying the apparatus to allow continuous and constant-rate fiber pulling.

Scale-up to produce research quantities of continuous fibers will be the primary goal of the proposed Phase II research. The scale-up design is based on the Phase I results. A preliminary cost analysis indicates a potential to produce mullite fibers for under $100/pound. The ability to produce larger quantities of fibers will allow the fibers and coatings to be optimized and tested in composites.

1. INTRODUCTION

This research demonstrated a new method for pulling fibers from undercooled melts by which high strength and chemically pure mullite fibers were obtained. The fibers and interface weakening coatings of YPO_4 demonstrated exceptional structural and chemical stability in a mullite matrix when the composite material was heated to 1500°C in air. The proprietary method of fiber pulling has application to a wide range of oxide materials and preliminary experiments to demonstrate YAG fiber pulling were successful. The results show that it would be feasible to produce fibers at relatively low cost, not only for mullite, but also for other oxide materials for which undercooling of the melt has been demonstrated.

This report presents the results of the Phase I SBIR project research. Further development of the method, the interface weakening coatings, and applications for the fibers are being proposed for the Phase II SBIR project.

1.1 Background

A new concept in fiber reinforced ceramic matrix composites (CMC's) is to coat fibers with an oxide material which is capable of undergoing a shear stress inducible martensitic transformation. If the coating is well bonded to the fiber and matrix, good strength properties are expected. For high toughness of the composite, however, the interfacial bonding should be weak to permit fiber-matrix debonding and fiber pullout. To date the latter has been achieved only by the use of graphitic carbon or boron nitride layers which allow easy slippage, but which are not chemically stable in an oxidizing environment.

By coating the fiber with an interfacial interphase of a transformable material where the transformation is accompanied by a negative volume change or large unit cell shape change, transformation weakening of the interphase should result. A "smart interphase" can thus be put in place such that the composite is capable of exhibiting both high strength in the absence of multiple matrix cracks, but also high toughness when a mechanism is able to be "switched on" locally should a crack propagate towards the fiber.

An alternative approach recently proposed by Morgan and Marshall at the Rockwell Science Center has been to apply an interfacial coating of monazite ($LaPO_4$). Being an oxide, it will not decompose in an oxidizing atmosphere, and it behaves in a chemically inert way to its "narcissistic" structure. Its inherent weak mechanical properties make it suitable as a simple weak interlayer to enable fiber pullout mechanisms and hence overall toughening of the composite. This mechanism should be able to operate up to the melting point of monazite at $\approx$ 2000°C.

Subsequently it has been recognized that yttrium phosphate (YPO_4) is an alternative attractive coating material. The present work has emphasized the synthesis of mullite fibers which were coated with YPO_4 and evaluated in a ceramic-ceramic composite. The mullite fibers

offer chemical stability, high strength, and the potential of high creep resistance at high temperature and are compatible with the YPO_4 coatings.

The developing opportunities in CMCs that result from these fiber coating concepts, can be exploited by (i) providing new oxide fiber materials that have properties suitable for CMC application and (ii) conducting detailed investigation of the fiber coating ideas to develop them towards CMC applications. The need for appropriate fibers creates the focussed business opportunity on which CRI has concentrated its efforts in the Phase I work. The need to guide fiber development toward application of the new fiber coating concepts has been met by collaborating with Professor W.M. Kriven of the University of Illinois at Urbana-Champaign (UIUC). The fiber properties, coating by pulsed excimer laser ablation (PELA), and performance in a ceramic-ceramic composite were investigated by Professor Kriven's research group.

1.2 Methods

The proposed research applied two different methods, one for fiber synthesis and the second for fiber coating, that have wide potential applicability in the processing of oxides. Melt drawing of fiber from undercooled melts was used for fiber synthesis, based on extensive research we had already performed [1-10] in the application of containerless melt processing of oxides. The pulsed excimer laser ablation (PELA) method was used for fiber coating, based on recent work [11,12] of Professor Kriven's group.

1.3 Markets and Applications

The opportunity and market for oxide fibers which motivated the Phase I research is in ceramic matrix composites (CMCs) that can be used at temperatures above *ca.* 1200°C, the upper limit for superalloys [13-16]. CMCs can replace superalloys in critical parts of heat engines, heat shields, thrust deflectors, and other components exposed to thermal and mechanical stress [13,14]. Use of CMCs will extend the operating temperature range of these components, increasing performance and efficiency.

Oxides were selected as the candidate materials to investigate the concept of drawing fibers from deeply undercooled precursor melts [6]. Deep undercooling below the equilibrium melting point increased the melt viscosity sufficiently to allow fiber pulling [5,6]. One goal of the Phase I research was to show that drawing could be used to make high strength oxide fibers by an economical route. The structure and properties of the fibers were measured and the effects of coatings on interfacial characteristics were investigated.

We anticipate that the research market will provide substantial short- to medium-term market for the fibers we have developed. This research market may be strongly supported by government agencies and aerospace firms who are the main driver for innovative high performance ceramic-ceramic composites applications. The Phase I research has demonstrated that small scale production of the oxide fibers is feasible and can be readily

developed to supply fibers for this market. Fiber prices less than $100/pound appear to be possible.

CRI is in the process of forming alliances to guide the Phase II fiber production and further development of interface-weakening coatings for composite materials. We will team with potential clients and fiber users during the Phase II research. A significant part of the Phase II proposal will be to supply fibers for R&D on applications so that the markets for these applications can be developed. Larger-scale commercial markets would be further developed in the early stages of the Phase III based on the advances in fiber production, coating, and applications achieved during the Phase II SBIR project.

2. PROJECT OBJECTIVES

The ultimate objective of CRI's efforts in oxide fibers is to manufacture and market oxide fibers that have the properties required for ceramic-ceramic composite materials applications. The Phase I research program was broadly designed to show that this objective is feasible. Important criteria of the ceramic-ceramic composite materials application were addressed during Phase I and they are discussed in section 3.7.

The specific goals of the Phase I work were to develop a process for making research quantities of oxide fibers by drawing from undercooled melts, characterize the fibers, and develop coatings which modify interfacial mechanical properties. The Phase I research objectives were to:

(1) Investigate containerless melting and undercooling of oxide materials selected for application to ceramic-ceramic composites.

(2) Demonstrate fiber drawing from undercooled melts for at least one of the selected materials and make research quantities of fibers.

(3) Apply coatings to the melt-drawn fibers that will toughen ceramic-ceramic composites formed from the fibers.

(4) Measure the structure and properties of as-drawn and coated fibers.

(5) Evaluate the costs for scale-up of the fiber growth and coating processes.

The project objectives were met and a new type of high purity mullite fiber was produced by pulling from undercooled liquid of the mullite composition. The fiber diameters were from 10-50 μm which was controlled *via* the melt viscosity (amount of undercooling) and the pulling rate. The microstructural, chemical and mechanical properties of the fibers were measured at the University of Illinois. The room temperature tensile strength of the mullite fibers was 5.61 $\pm$ 0.71 GPa.

Longer-term efforts to establish markets for commercial quantities of fibers will require continuous fibers supplied in the form of tows or other forms such as tapes or pre-preg that are widely used in the manufacture of composite materials. We intend that the commercial stage of the enterprise will be in collaboration with partner companies who are users, manufacturers, and/or suppliers of composite materials.

3. WORK PERFORMED AND RESULTS

The Phase I SBIR research was performed at CRI in Evanston, Illinois, and at the University of Illinois, Urbana-Champaign under a subcontract.

The work at CRI focussed on developing the innovation - drawing fibers from molten oxides that were undercooled below their melting point to increase the melt viscosity. This work is described in the first three sections below. The work at UIUC was directed by Professor W. M. Kriven and focussed on microstructural, chemical, and mechanical characterization of the fibers and the investigation of interface-weakening fiber coatings. This work is described in Section 3.4 and 3.5. The combination of high strength fibers and interface-weakening coatings provide both strength and toughness in composite materials. Section 3.6 discusses scale up and presents a preliminary fiber production cost analysis. Section 3.7 discusses market research to guide commercial development of the technology.

3.1 Materials

Materials were chosen for their capability to provide high temperature strength, high modulus, chemical stability in oxidizing environments, creep resistance, and compatibility with the interface-weakening coatings. Mullite compositions in the alumina-silica system were chosen for detailed investigation. Preliminary experiments were also performed with the YAG (yttrium-aluminum garnet) composition which is also known to have high potential for creep resistance at high temperatures.

The materials were chosen in part based on our previous experience with aluminum oxide, alumina-silica, and alumina-yttria compositions in containerless experiments. We have already shown in previous work [6,8-10] that considerable undercooling of aluminum oxide and aluminates can be achieved. It is known that the viscosity of these liquids increases significantly as the temperature decreases, and it was hypothesized that undercooling below the melting point would provide a sufficient viscosity to support fiber pulling. In some cases, *e.g.*, the YAG and mullite compositions, glass formation has been achieved in containerless undercooling experiments [10].

The temperature-viscosity relationships for several alumino silicates were measured by Urbain, *et al.* [18,19]. Figure 1 shows a plot of log viscosity *vs* inverse temperature obtained by extrapolating the functions from Urbain, *et al.* [19] to lower temperatures. In earlier work we showed that aluminum oxide can be undercooled by *ca.* 17% of its absolute

melting point [6]. The slope of the viscosity-temperature relationship may also depend on melt composition and processing history.

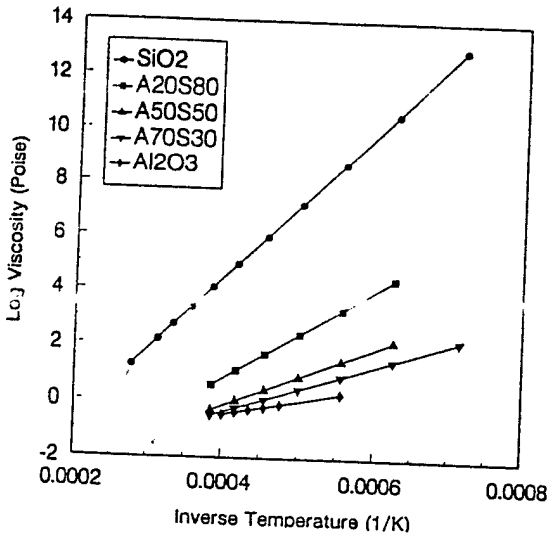

Figure 1. Plot of log. viscosity *versus* inverse temperature for the molten alumina, silica, and alumino-silicates containing 20, 50 and 70 mole % silica [19].

The materials selected to investigate fiber growth from the melt are given in Table I. The 60/40 alumina-silica composition is stable 3:2 mullite. The 70/30 alumina-silica composition is near the composition limit of "metastable" mullite [20]. The 63/37 alumina-yttria composition is the yttrium aluminum garnet (YAG) phase.

Table I. Alumina-based binary compositions used for fiber drawing experiments.

Mole fraction Al_2O_3	Mole fraction SiO_2	Mole fraction Y_2O_3
0.60	0.40	0
0.67	0.33	0
0.69	0.31	0
0.70	0.30	0
0.63	0	0.37

Initial experiments were performed using samples that were synthesized by laser hearth melting [21] from the pure oxides. Later experiments, including all of the fiber growth experiments for which property measurements, fiber coating, and high temperature testing were performed used samples made from "Kyoritsu" mullite [22]. This is a high purity mullite formed by sol-gel processing methods. In all cases, samples of the mixed oxide powders, or the pure "Kyoritsu" mullite were melted in the laser hearth to form *ca.* 0.3 cm diameter dense and nearly spherical specimens that were subsequently used in the levitation melting and fiber pulling experiments.

3.2 Containerless Processing of Oxide Melts

Containerless melt processing eliminates contamination of materials by containers and container-induced nucleation of crystalline phases when melts are cooled below their melting points or liquidus temperatures. As a result, deep undercooling is achieved with increased melt viscosity to facilitate fiber drawing.

The methods we used for containerless melt processing are (i) aero-acoustic levitation (AAL, Figure 2) [5] and (ii) conical nozzle levitation (CNL, Figure 3) [23]. Both methods employ aerodynamic forces to levitate samples which are laser heated and melted using a CO_2 laser of up to 500 watts.

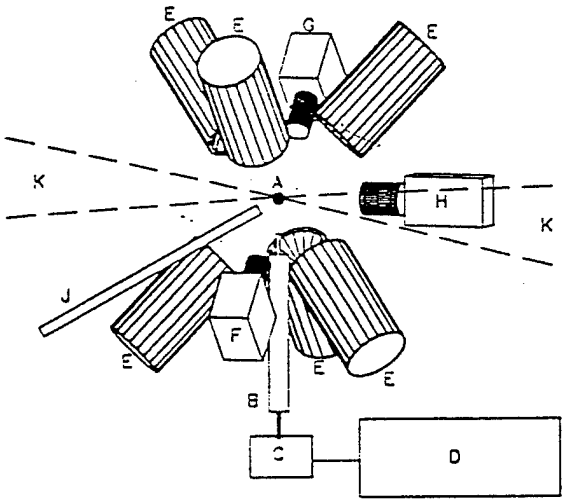

Figure 2. Schematic of the aero-acoustic levitator. A, specimen; B, gas flow tube; C, translation stage; D, flow control system; E, acoustic transducers; F, specimen illuminator; G, position detector; H, video camera; J, vacuum chuck; K, laser beam.

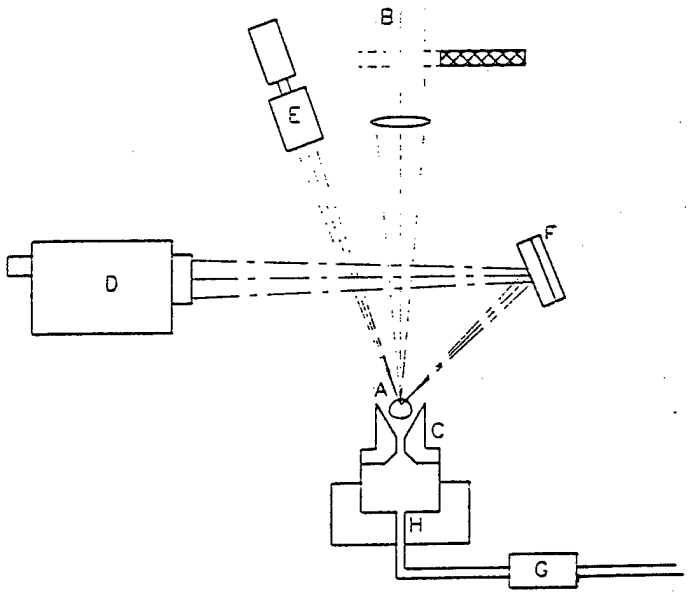

Figure 3. Schematic of conical nozzle levitator. A, specimen; B laser beam; C, nozzle; D, Pyrometer; E, video camera; F, mirror; G, gas flow controller; H, plenum chamber.

In aero-acoustic levitation [5], the levitated sample is stabilized by acoustic forces generated by an array of six high frequency (ca. 22,000 Hz) transducers. The acoustic forces are sufficient to levitate low density liquids such as water. Acoustic phase differences between opposed transducers are controlled to stabilize the sample position when the sample shape and aerodynamic forces change or fluctuate. The open geometry of the AAL apparatus allows quite uniform temperatures to be achieved by laser beam-heating the levitated specimen from two sides. The levitation gas flow induces rapid stirring of liquid specimens, which also helps achieve a uniform temperature. The phases of the acoustic signals can be adjusted to reduce aerodynamic stirring and the laser illumination can be adjusted to obtain increased temperature gradients in levitated melts.

Conical nozzle levitation [23] is simpler than the AAL method and is much less costly to set up and operate. CNL uses aerodynamic forces alone, with the sample contained in a shaped nozzle which provides a strong axial variation in the levitation force. Only minor variations in position occur upon melting or with specimen shape changes.

The sample materials were levitated, melted, and undercooled. The fibers were drawn from the undercooled melts as described in the next section. The method is applicable to additional oxide materials; we have demonstrated deep undercooling and in some case, glass formation, of pure aluminum oxide [6], alumina-silica compositions [10], zircon ($ZrSiO_4$) [24], bismuth copper oxide and bismuth gallium oxide eutectic mixtures [24], yttrium-barium-copper oxide superconductor materials [3,4,7], and calcia-gallia [2] mixtures.

3.3 Fiber Drawing

Fibers were drawn from levitated molten oxide drops about 0.3 cm in diameter. The first experiments were performed in the aero-acoustic levitator to establish process conditions under which fiber drawing was possible. Later experiments used the conical nozzle levitator (CNL). In both cases, the fibers were drawn from a location at the side of the specimen, in a direction approximately normal to the vertical gas flow that supported the levitated liquid. The radial restoring forces in the levitators are quite small so that the pulling force was limited. Arrangements to pull the fibers in a direction opposite that of gas flow would allow fiber pulling at lower temperatures and greater rates than were achieved in the Phase I research.

The aero-acoustic levitator provided wide optical access to the levitated specimen and used dual beam heating to reduce temperature gradients in the liquid. This method allowed a wide range of processing conditions to be investigated. It also allowed more accurate temperature measurements than were possible in the conical nozzle levitator.

The conical nozzle levitator used single laser beam heating, resulting in large temperature differences between the laser beam-heated top side and the aerodynamically-cooled bottom side of the levitated liquid drops. The CNL was a more convenient device for fiber-making than the AAL instrument. It is proposed for Phase II to use the sample temperature

gradients that occur in the CNL to draw fibers from the undercooled liquid at the bottom, while maintaining the top of the specimen at a temperature above the melting point where added material can be melted. The CNL thus provides the ability to achieve continuous fiber growth. It permits increased fiber pulling rates by directly opposing the fiber drawing and levitation forces.

The procedure was to levitate a solid specimen, melt it by heating it with a focussed laser beam, undercool the liquid by blocking the heating beam, introducing a stinger into the melt and withdrawing the stinger to form a fiber. The stinger briefly contacted the liquid so that the tip of the stinger was wetted and fiber pulling was initiated. Stingers were made from 2.5 cm. lengths of tungsten, platinum, or sapphire. Tungsten and platinum stingers were 75 μm diameter and the sapphire stingers were 100 μm diameter.

The experimental setup of the stinger and fiber drawing apparatus is illustrated in Figure 4. The stinger was fixed to the fiber pulling mechanism with a delrin ferrule. The mechanism incorporated a solenoid to insert the stinger into the molten drop and retract the fiber. After research with different mechanisms, the apparatus was modified so that the pulling rate was controlled with a spring or a falling weight and a friction damper. The residence time of the stinger in the liquid was set by controlling the time for which the solenoid was activated. The residence time could be varied from 0 to 100 milliseconds.

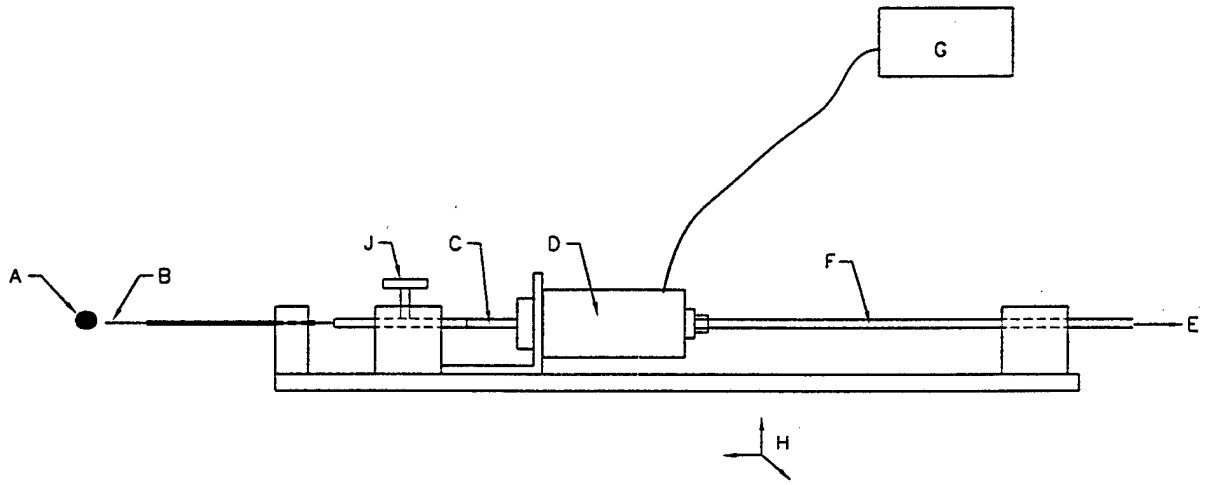

Figure 4. Schematic illustration of the fiber pulling stinger system. A - levitated liquid drop; B - stinger (1 cm length of 75 μm tungsten wire); C - stinger holder; D - solenoid actuator; E - spring or falling weight; F - pulling rod; G - solenoid control electronics; H - x-y-z translation stage; J - friction damper.

The fiber pulling apparatus was mounted on an x-y-z translation stage used for precise positioning of the stinger relative to the liquid drop. During setup, the fiber pulling

apparatus was positioned so that the stinger was about 0.5 cm from the surface of the drop. Adjustment of this distance allowed the penetration depth into the liquid to be varied in the preliminary experiments. The penetration depth used to draw fibers was in the range 0.1 to 1.0 mm.

In order to investigate fiber drawing as a function of the melt temperature, the fibers were drawn during transient cooling of the liquid drops initiated by blocking the heating laser beams. The melt was first heated and held at a fixed initial temperature slightly above the melting point. The heating laser beams were blocked to initiate cooling of the melt and the fiber drawing device was activated after an elapsed interval of time. By changing the time interval, fiber drawing was achieved as a function of the melt temperature, i.e.; the degree of undercooling. The fiber lengths were 1-2 cm in these experiments and fiber drawing occurred at a rate of approximately 30 cm/s. Melt cooling rates were approximately 300°C/s, so that the melt temperature varied by 10-20°C during the fiber drawing event.

The liquid drop temperature was measured with an optical pyrometer and the temperature *vs* time data were acquired with a computer. Figure 5 shows a typical cooling curve for mullite. The liquid was heated and held at a temperature of *ca.* 2000K. At 20.5 seconds on the plot, the heating beam was blocked and the liquid cooled below its equilibrium melting point. At *ca.* 22 seconds, the undercooled liquid spontaneously recrystallized, reheating the drop to its melting temperature. Thus, the time interval used to investigate fiber drawing as a function of temperature was in the range 0 - 2 seconds after cooling of the liquid was initiated.

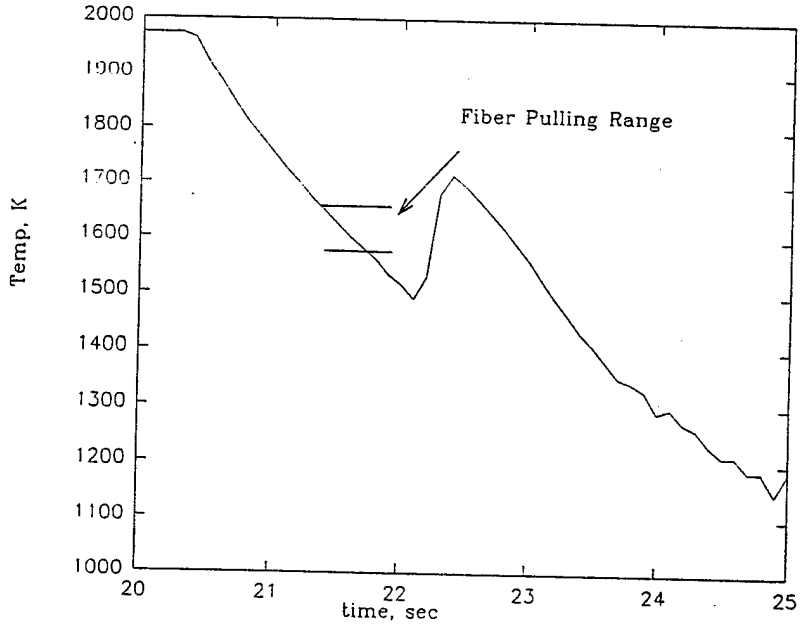

Figure 5. Typical cooling curve for a 0.3 cm diameter mullite specimen levitated and melted in an aero-acoustic levitator. The preferred temperature range for drawing fibers is marked on the figure.

The preferred temperature range for drawing fibers was approximately 70-140°C below the melting point. At higher temperatures, rather short fibers were obtained or the stinger pulled from the melt without drawing a fiber. At lower temperatures, the fiber drawing force tended to pull the entire sample from its levitated position.

The sample temperature-time plot was displayed in real time on a computer monitor. The display provided a convenient way of manually timing the stinging and fiber pulling. Fiber pulling was typically performed when the drop was cooled to an apparent temperature of 1580 to 1650K, *i.e.*, about 70 to 140K below the melting point. Fibers were also pulled at temperatures outside this range in a few experiments.

Liquid mullite could be maintained for a long period of time in the undercooled state used for pulling fibers. The CNL apparatus required that the correct temperature occur at the side of the liquid drop from which the fibers were drawn, while the bottom of the specimen was at a significantly smaller temperature. Therefore, the transient method was used for making fibers in the CNL, so that difficulties with the spontaneous crystallization would not occur. This transient method will not be required when the apparatus is modified to allow fiber drawing from the bottom of the liquid drop, to achieve continuous fiber pulling with the CNL apparatus.

Process variables which were investigated in the fiber pulling research were: (i) melt composition, (ii) melt temperature during pulling, (iii) stinger material, (iv) stinger residence time and penetration depth in the melt, and (v) pulling rate. Preliminary experiments were also performed to investigate fiber drawing from molten mullite in pure oxygen, air, or an inert-argon gas environment. Operation in air or oxygen was selected for all of the experiments to make fibers for testing.

3.3.1 Results of Fiber Pulling Experiments

Table II presents the results of fiber pulling experiments. The results of fiber growth experiments are given in columns 1-6 of the table. The first column shows fiber numbers for accounting purposes. Entries in the second column give the melt compositions listed earlier in Table I, or "mullite" for the experiments using Kyoritsu mullite [22] as the specimen material. The third column gives the apparent temperature of the undercooled liquid at the moment that pulling of the fiber was initiated. The apparent temperatures were measured with an optical pyrometer and were slightly smaller than the true liquid temperatures because the spectral emissivity of the liquid was less than unity. Column 4 gives the ambient gas in which the liquid was levitated. Columns 5 and 6 give the length and diameters of the fibers that were obtained. The cases where two or three diameters are given for a single fiber correspond to measurements on tapered fibers near the stinger, in the middle, and near the end of the fiber. Single diameter measurements are reported for fibers of more uniform diameter. Five fiber diameter measurements are given to 0.1 μm and correspond to measurements on the fracture cross section after tensile testing.

Table II. Results of Fiber Pulling Experiments

No.	Melt Comp.	Pulling Conditions Temp, C	Gas	Length mm	Diameter Micrometers	Al/Si Ratio by EDS SEM-EDS	TEM-EDS	Tensile Str., GPa
2	70%		air	4		4.70		
3	60%		air	3				
6	60%	1400	air	4				
7	67%	1500	air	4				
8	69%	1500	air	4				
9	69%	1400	air	4				
10	69%	1450	oxygen	4				
12	70%	1475	air	1	23, 11, 1			
14	70%	1500	air	1	20, 10, 1			
19	mullite	1400	oxygen	25	15		1.67	
20	mullite	1400	oxygen	24	54, 37, 2			
22	mullite	1400	argon					
23	mullite	1400	argon					
24	mullite	1400	argon					
25	mullite	1400	air	40	32.0			6.450
26	mullite	1400	air	33	21		2.10	
27	mullite	1400	air	60	20.5			4.684
29	mullite	1400	air	60	28	3.65		
30	mullite	1400	air	35	30	3.04		
31	mullite	1400	air	45	30			
32	mullite	1400	oxygen	35	43	2.62		
34	mullite	1400	oxygen	35	45			
35	mullite	1450	oxygen	20				
37	mullite	1420	oxygen	53	32.7			5.213
39	mullite	1500	oxygen	6				
40	mullite	1325	oxygen	52	60	3.31	1.77	
42	mullite	1275	oxygen	49	30.5			6.142
43	mullite	1275	oxygen	40	33.0			5.550
44	70%	1400	oxygen	30	35	4.94		
						Average:		5.608
						Standard Deviation:		0.708

Table III. Calibrations for Fiber Composition Measurements

No.	Sample Composition Alumina	Silica	Al/Si Ratio by EDS SEM-EDS	TEM-EDS
3:2	60.0%	40.0%	3.72	2.01
2:1	66.7%	33.3%	4.30	
3:1	75.0%	25.0%	4.60	4.78
3:1	75.0%	25.0%		3.66
3:1	75.0%	25.0%		3.30

Property measurements on selected fibers are also given in Table II. These property measurements are described and discussed later. Table III presents the results on calibration standards for fiber composition measurements.

3.3.2 Conditions for Fiber Pulling from Undercooled Melts

The demonstrated conditions for pulling mullite fibers represent the key information required to (i) make the specimens used in the fiber property measurement and fiber coating research, and (ii) design scaled-up fiber production that will be required in the Phase II research and commercialization of our process. This subsection summarizes these key results of the Phase I project. The conditions under which mullite fiber pulling was demonstrated and related conclusions that will be important in further work are presented and discussed below. Extension of the method to additional materials is also discussed.

1. Melt temperature and viscosity for pulling fibers

   The fibers were successfully pulled from melts undercooled by 70-140°C below the melting point. From the data of Urbain [19], the viscosity was estimated to be 100 to 200 Poise in this temperature range. Considerably larger viscosities occur in glass fiber drawing operations, in which the drawing rates are greater than the 30 cm/s rates achieved in this work. It can be seen from Figure 5 that increased undercooling (lower temperatures) and larger viscosities are available in the undercooled mullite melts. The pulling of fibers at greater rates will be facilitated by drawing the fibers from the bottom side of liquid drops levitated in the CNL. Much larger pulling forces can be sustained in this alternative geometry because the fiber pulling and levitation forces will be directly opposed.

2. Stinger Preparation

   The stinger needs to be "primed" by wetting it with the material which was being pulled. Priming was achieved by activating the fiber pulling device several times with the liquid drop maintained at a temperature near or slightly below the melting point. Fibers were not formed under this condition, but a slight coating of mullite was formed on the stinger surface. The best results were obtained with a tungsten stinger.

3. Stinger Operation

   The residence time of the stinger in the undercooled drop needs to be controlled to (i) avoid stinger-induced crystallization of the entire drop and (ii) achieve wetting of the stinger to allow fiber drawing. The optimum residence time was 10-20 ms.

4. Fiber Pulling Rate

The fiber pulling rate was controlled to exceed the crystallization velocity of the undercooled melt in the successful fiber-pulling experiments. The crystallization velocities were not precisely known as a function of temperature. For mullite fibers, a fiber pulling rate of 30 cm/s was sufficient to avoid melt crystallization. Video images of a liquid drop crystallized by contact with the stinger showed the crystallization velocity to be *ca.* 3 cm/s at 200K below the melting point.

Experiments with YAG fiber growth showed the crystallization velocity to be significantly greater for liquid YAG than for liquid mullite. YAG fibers of a few mm in length were drawn at 30 cm/s before crystallization of the melt occurred. Detailed investigation of YAG fiber drawing was not performed. It was evident that a pulling apparatus to achieve increased pulling rates will be required for YAG fiber growth.

The use of containerless processing allowed deep undercooling so that a melt viscosity sufficient to draw fibers was obtained. Many other oxide materials have also shown this deep undercooling that permits fiber pulling. Examples include Al_2O_3, $ZrSiO_4$, $CaAl_2O_4$, ceramic superconductor materials, and others. Fiber pulling experiments would be required to demonstrate the feasibility of fiber growth from these undercooled melts. The key requirement will be not only that a large undercooling is achieved, but also that a sufficient viscosity occurs to allow fiber pulling at high rates. Glass formation in containerless cooling experiments on $CaAl_2O_4$ and several other oxide materials has already demonstrated that high viscosity occurs in the undercooled liquids.

The need to extract fibers at a high rate to prevent the stinger from inducing crystallization of the undercooled drop means that the fiber pulling rate must be inherently fast. The fiber diameter is a function of fiber pulling rate and the melt viscosity. The diameter of fibers pulled with the spring-operated mechanism decreased as the fiber length and the pulling rate increased during the process. Use of the damper mechanism allowed a more uniform pulling rate and fiber diameter. Development of continuous fiber pulling would allow fibers to be drawn with extremely uniform diameters.

Approximately 150 mullite fibers of 5 to 15 cm in length were made in the CNL. The pulling method was optimized using tungsten stingers. Fiber pulling was accomplished by a actually 44,000 dyne/cm tension spring which was extended by approximately 15 cm. The spring operated against a friction damper so that the pulling velocity was limited to approximately 30 cm/s.

3.4 Characterization

The work to characterize fibers was directed by our consultant, Professor W.M. Kriven of the Department of Materials Science and Engineering, University of Illinois at Urbana-Champaign. Facilities at UIUC were used for the measurements. Dr. Mohammed Jilavi

performed microstructural and chemical measurements. Dr. Dong Zhu performed mechanical property measurements.

3.4.1 Microstructural Characterization

Microstructural characterization included scanning and transmission electron microscopy and electron diffraction measurements of the structure of crystalline regions.

Scanning electron microscopy was used to evaluate the surface morphology, the diameter of fibers along their length, and the chemical composition of the fibers. In the early feasibility experiments, fibers were drawn at a rate which increased as the fiber was pulled. The resulting fibers were tapered along their length. Figure 6a and 6b show regions along the length of a fiber pulled at a rate that increased from 5 to 30 cm/s as the fiber was pulled. The diameter of the fiber decreased from approximately 20 μm where it touched the stinger to 1 μm at the tip.

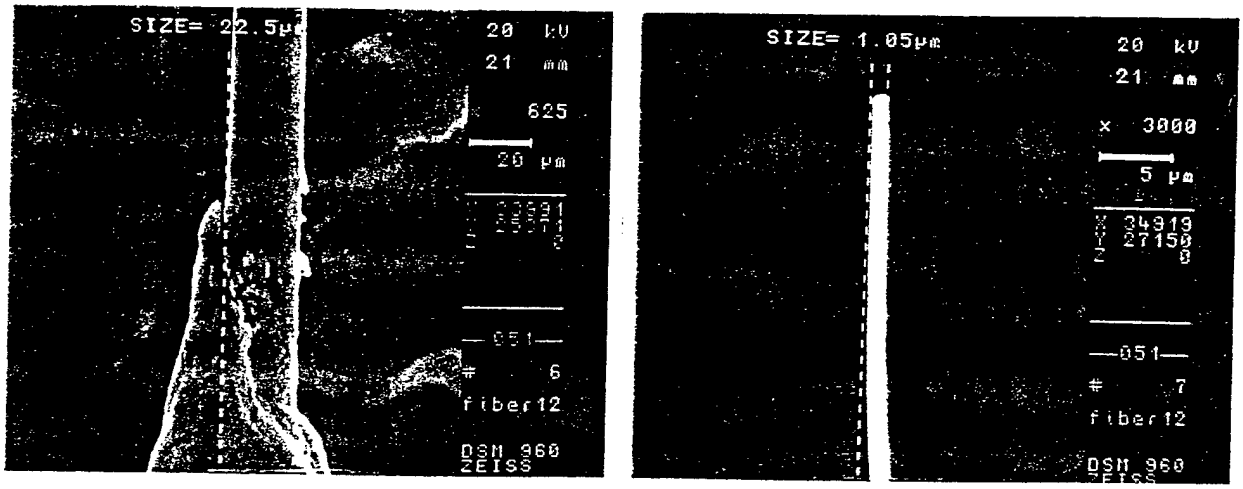

Figure 6. Scanning electron micrograph of a 70 mol% aluminum oxide fiber pulled in air from a drop of liquid undercooled to *ca.* 1725 K. The fiber was approximately 1 cm in length. Left: A section of the fiber that grew near to the stinger. Right: the tip of fiber.

Figure 7 is a scanning electron micrograph of a mullite fiber surface. The fiber surface was smooth, homogeneous and free from imperfections. SEM examination showed that the fibers exhibited glassy fracture to produce smooth and dense fracture surfaces.

Fibers made from stoichiometric 3:2 alumina:silica mullite were examined in a Philips CM12 transmission electron microscope. Figure 8 shows a transmission electron micrograph of a thinned section of a mullite fiber. A representative electron diffraction pattern is also shown in the figure. The diffraction rings obtained by selected area diffraction (SAD) at several

points on the fiber were diffuse indicating that the fiber was amorphous. The absence of extinction contours and grain boundaries showed that the material was amorphous.

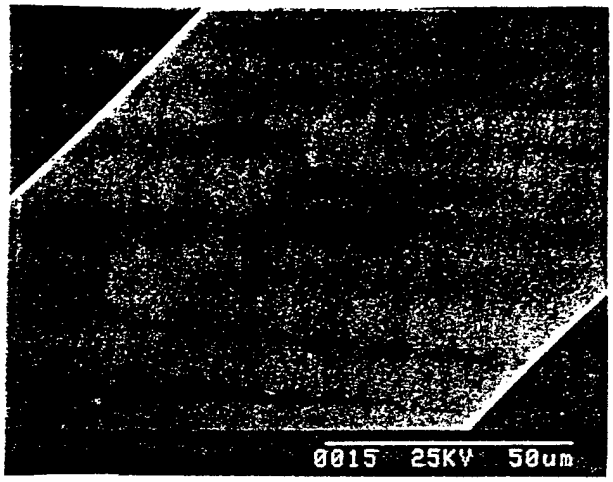

Figure 7. Scanning electron micrograph of a 3:2 mullite fiber. The fiber surface was smooth, homogeneous and free from imperfections. The fiber was pulled in oxygen from a drop of liquid undercooled to *ca.* 1675 K.

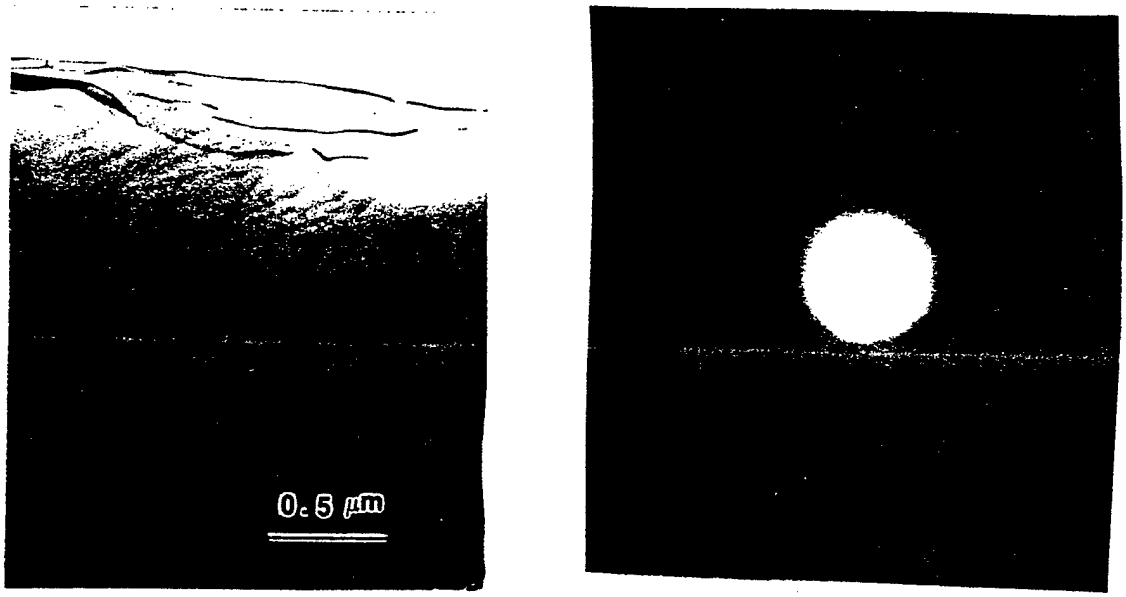

Figure 8. Transmission electron micrograph (left) and electron diffraction pattern (right) from a mullite fiber. The specimen surface ripples are artifacts from the ion milling operation used to prepare the specimen. The diffuse diffraction pattern indicates that the material is amorphous.

3.4.2 Chemical Characterization

Chemically inhomogeneous regions were occasionally found near the ends of the fibers or in the fibers of 70% composition that were drawn during the initial experiments. Figure 9 illustrates the inhomogeneous areas in a fiber from these early experiments. Occasional branching of the fibers was also observed, as illustrated in Figure 10. These effects were observed in fibers drawn at relatively high temperatures and of the 70% Al_2O_3 composition. Fibers obtained from the 60% (mullite) composition and at somewhat lower drawing temperatures did not exhibit these effects.

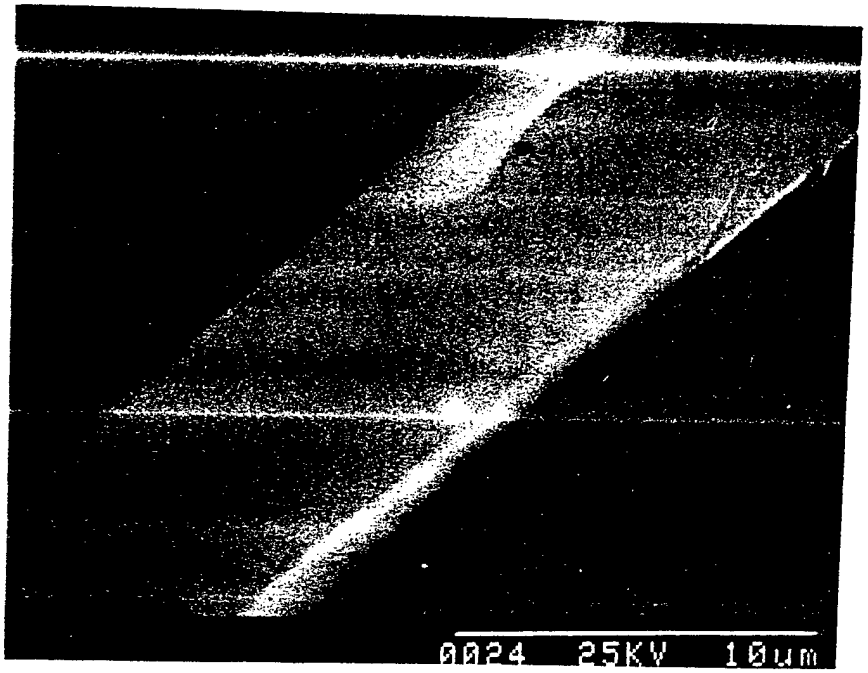

Figure 9. SEM micrograph of fiber No. 14 showing apparent phase separation. This fiber was pulled in air from a melt of 70 mol% Al_2O_3 at 1500°C. The melt was heated extensively prior to fiber pulling, and may have experienced a composition change due to vaporization of its components.

Heating and melting of the samples prior to drawing of the fibers was usually performed in a few minutes, and the levitated sample lost less than 1% of its mass during this period. Little or no melt composition change could occur prior to drawing of the fibers. After recrystallization of the amorphous fibers that were drawn from molten mullite, crystalline mullite was detected by x-ray diffraction, and no glassy or other crystalline phases were detected by SEM and TEM.

The normalized ratio of the Al:Si signal intensity measured by SEM/EDS and TEM/EDS on standard specimens of known composition and on selected fibers were presented in Tables II and III. The EDS results for fibers grown from liquid drops of the mullite (60% Al_2O_3)

composition showed a slightly smaller Al:Si intensity ratio than the calibration standard. Considerable scatter in the results on the order of $\pm$10-15% occurred in the Al:Si intensity ratios. Significant corrections would be required to calculate compositions from these measurements since the calibration specimens were flat but the fiber surfaces were curved. The orientation of the spot on the fiber surface relative to the EDS detector was therefore variable (and not determined) leading to different absorption corrections for each of the fiber composition measurements. The results are within the expected agreement for fibers and calibration materials of equal composition. They thus show than no gross departures from the liquid drop composition occurred during the fiber drawing process.

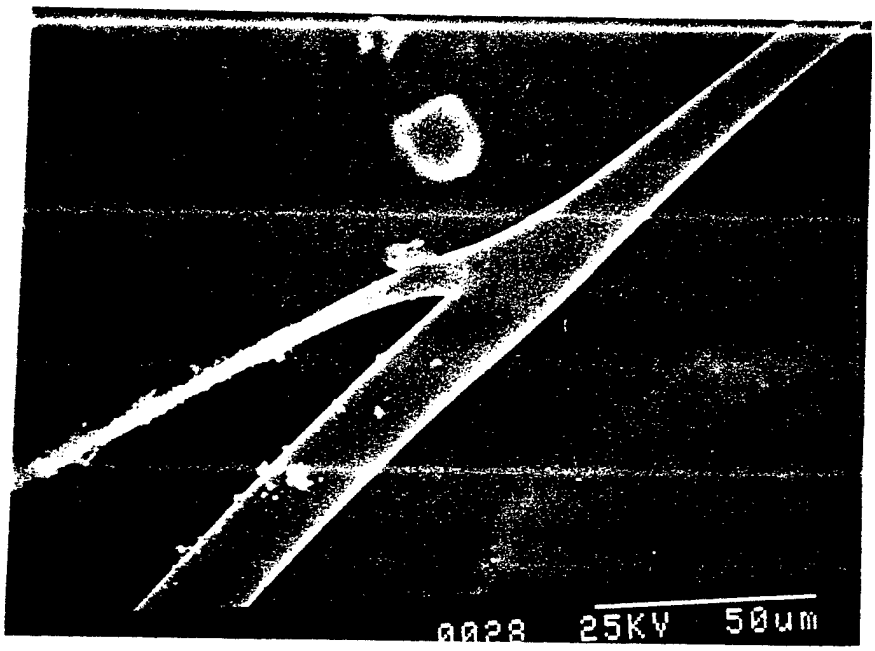

Figure 10. SEM micrograph of fiber No. 12 showing branches seen infrequently in the fibers. This fiber was pulled in air from a melt of 70 mol% Al_2O_3 at 1475°C.

The SEM and TEM results showed the fibers to have a uniform appearance and without any atomic number contrast that would occur if the fiber composition was not uniform. It was concluded that the fibers were of a uniform composition which was nominally equal to that of the melt from which the fibers were drawn.

3.4.3 Mechanical properties

Properties determined by measurements on single fibers provide a useful way to evaluate new materials. It was well know that the mechanical properties of fine filaments are very different from the bulk properties of the same materials. The difference comes from not only the material properties (e.g. microstructure, defects in unit volume of structure, orientation of crystal, etc.), but also the testing method.

The fiber strength was measured using a method developed at UIUC for high-modulus single-filament materials. The fiber diameters were 20-30 μm, the gauge length was fixed at 23 mm, approximately 1000 times the fiber diameter. Test fibers were bonded into a specially designed frame with "M-Bond" epoxy adhesive. The measurement technique and interpretation was consistent with ASTM standard D3379-75. Tests were performed in an Instron 1205 tensile testing machine operated under computer control. Fibers were pulled at a constant strain-rate = 5 μm/s. A high sensitivity load cell was used to measure load.

A computer was used to record the load and displacement as a function of time. Broken fibers were examined by optical microscopy to determine the cross section so that stress could be determined.

Several mullite fibers were tested at ambient temperature. A representative stress-strain plot for a mullite fiber is presented in Figure 11.

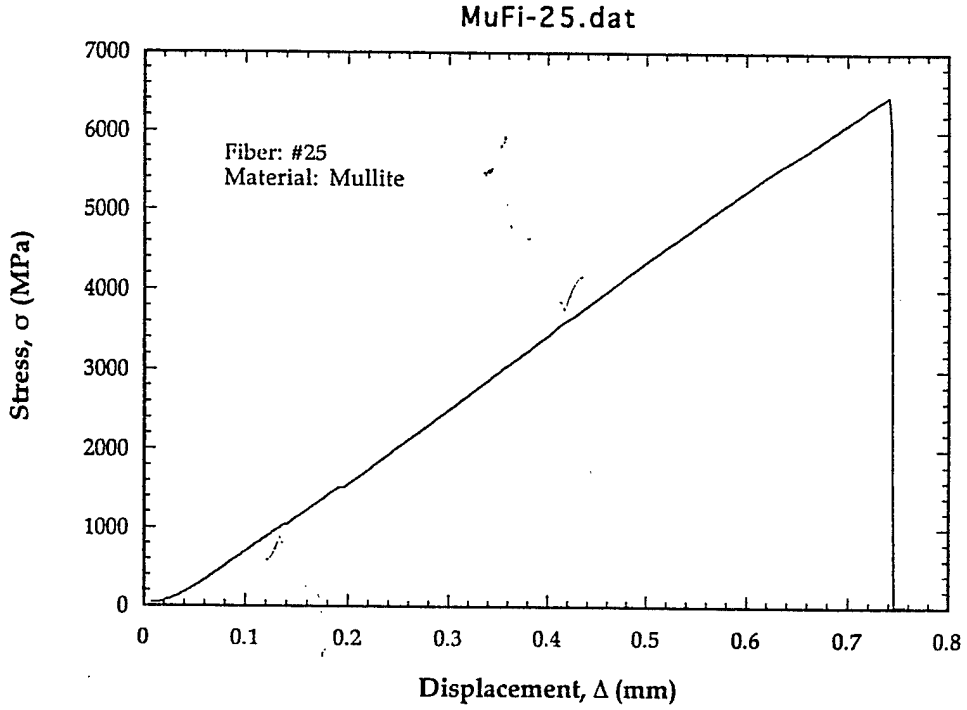

Figure 11. Load-displacement plot for mullite fiber Number 25 pulled at a strain rate of 5μm/s at ambient temperature.

The mean tensile fracture strength of five fibers was 5.61 $\pm$ 0.71 GPa. Fibers were typically amorphous and contained few defects and flaws. The small number of flaws is advantageous since it provides more consistent mechanical properties.

Table IV summarizes the results of fiber tensile tests, including measurements on crystallized fibers that are discussed in the next section.

Table IV. Mullite Fiber Mechanical Testing Results

Fiber Number	Condition	Diameter, μm	Strength, GPa
25	As-Pulled, amorphous	32.0	6.45
27	As-Pulled, amorphous	20.5	4.68
37	As-Pulled, amorphous	32.7	5.21
42	As-Pulled, amorphous	30.5	6.14
43	As-Pulled, amorphous	33.0	5.55
	Crystallized at 1100°C	19	0.78
	Crystallized at 1200°C	8	1.00
	Crystallized at 1200°C	28	0.66

3.4.4 Recrystallization

The mullite fibers were annealed in air at different temperatures for 1 hour. Annealing conditions and results are given in Table V.

In order to test if the fibers could be used at high temperatures, 1500°C annealing was first conducted. The fiber was placed on Pt foil for heat treatment in air, and after annealing, it shrunk and broke into several pieces. The fiber became brittle and could not be picked up with tweezers. After 1300°C annealing, the fiber kept its shape, but broke when handled with tweezers.

Table V. Procedures for annealing mullite fibers

Temperature	1500°C	1300°C	1200°C	1100°C
Soak time, hr	1	1	1	1
Heating and cooling rate	5°C/min	5°C/min	5°C/min	5°C/min
Result	Broken into several pieces	Broken when picked up with tweezers	One broke when installed in test machine	One was OK, the other failed to test

After 1200°C annealing, the fibers were mounted on a plastic frame using epoxy. One of three fibers broke during the installation for tensile testing. The failure was caused by the curvature of the fiber, where the bending force resulted in fiber breakage during installation. Tensile tests were successful on the other two fibers.

Several fibers were annealed at 1100°C. Only two of these fibers were long enough to mount for tensile testing. One of these fibers had a non-uniform diameter and broke without obtaining a tensile test.

Figures 12 and 13 present the stress *vs* displacement curves for two fibers that were annealed at 1100°C and 1200°C, respectively. The tensile strengths measured for crystallized fibers are presented in Table IV.

Fibers annealed at 1200°C were examined by TEM. Figure 14 shows that the microstructure was polycrystalline with a sub-micron grain size. Selected area electron diffraction (SAD) of individual grains given in Figures 15 and 16 were indexed as stable 3 $Al_2O_3 \cdot SiO_2$ mullite. This was confirmed by microchemical analysis using energy dispersion X-ray spectroscopy (EDS) in the TEM.

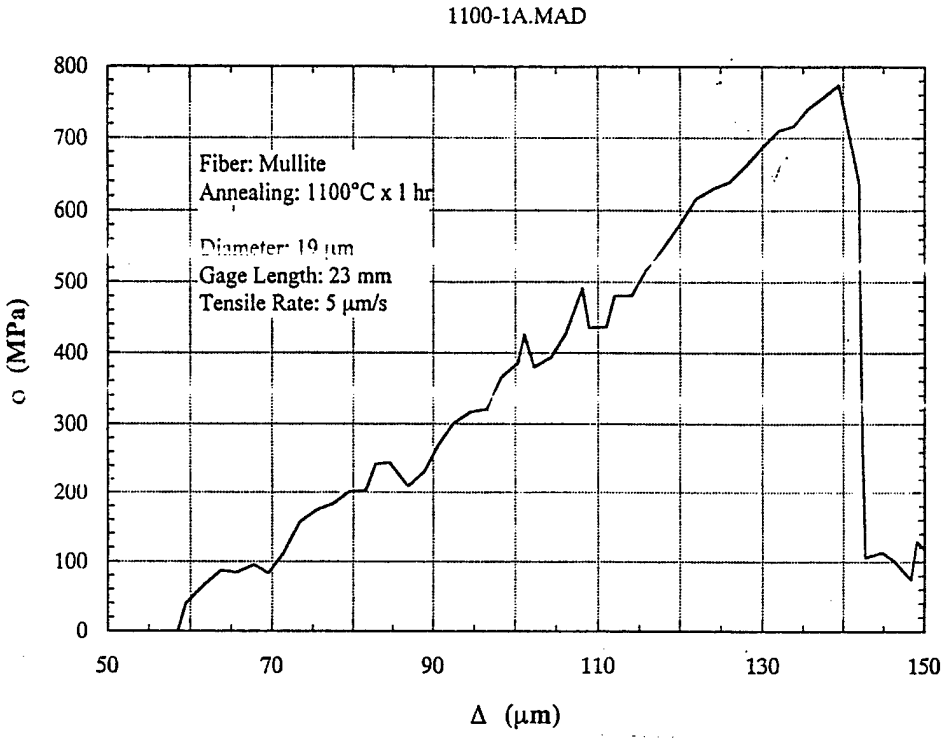

Figure 12. Stress *vs* displacement curve for a fiber annealed and crystallized at 1100°C.

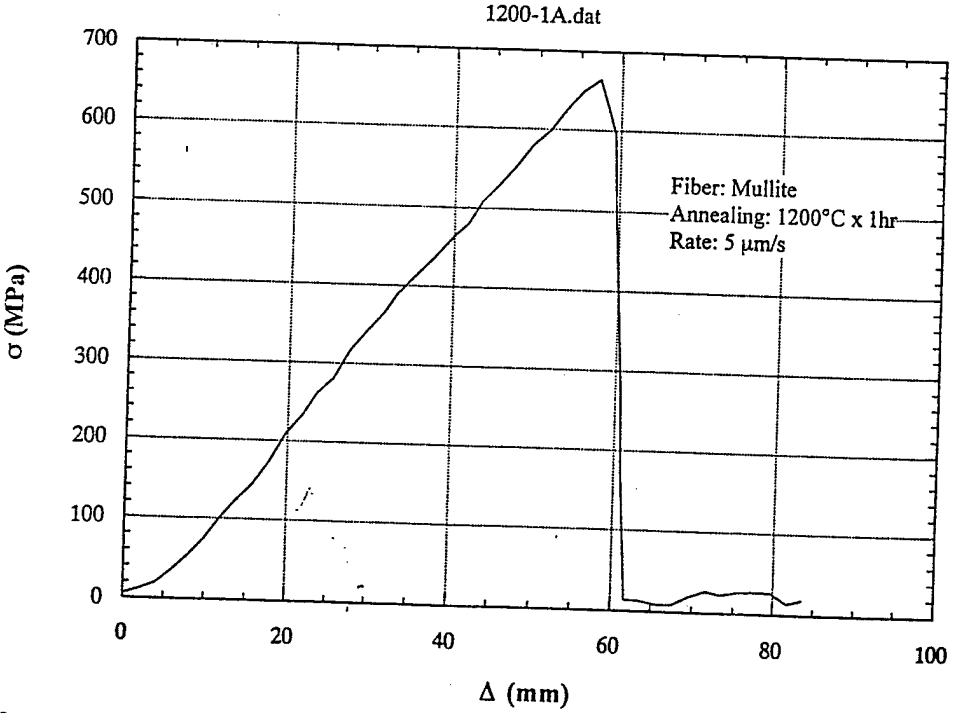

Figure 13. Stress *vs* displacement curve for a fiber annealed and crystallized at 1200°C.

Figure 14. Bright field TEM micrograph of polycrystalline mullite fiber annealed at 1200°C for one hour in air.

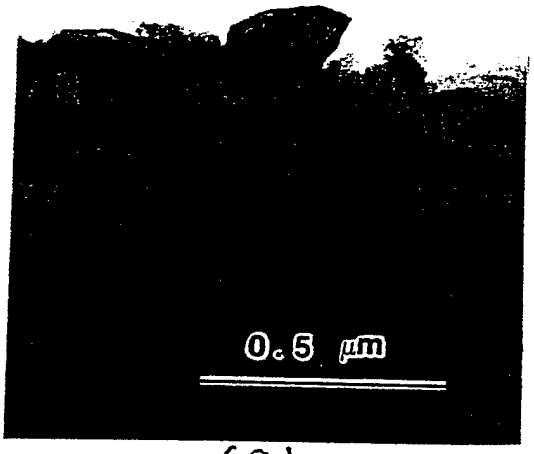

(a)

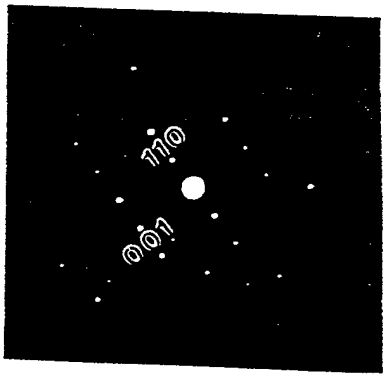

(b)

Figure 15. (a) Bright field TEM micrograph of an individual mullite grain and (b) corresponding selected area diffraction pattern indexed as 3 $Al_2O_3 \cdot SiO_2$ mullite in the $[1\bar{1}0]$ zone axis.

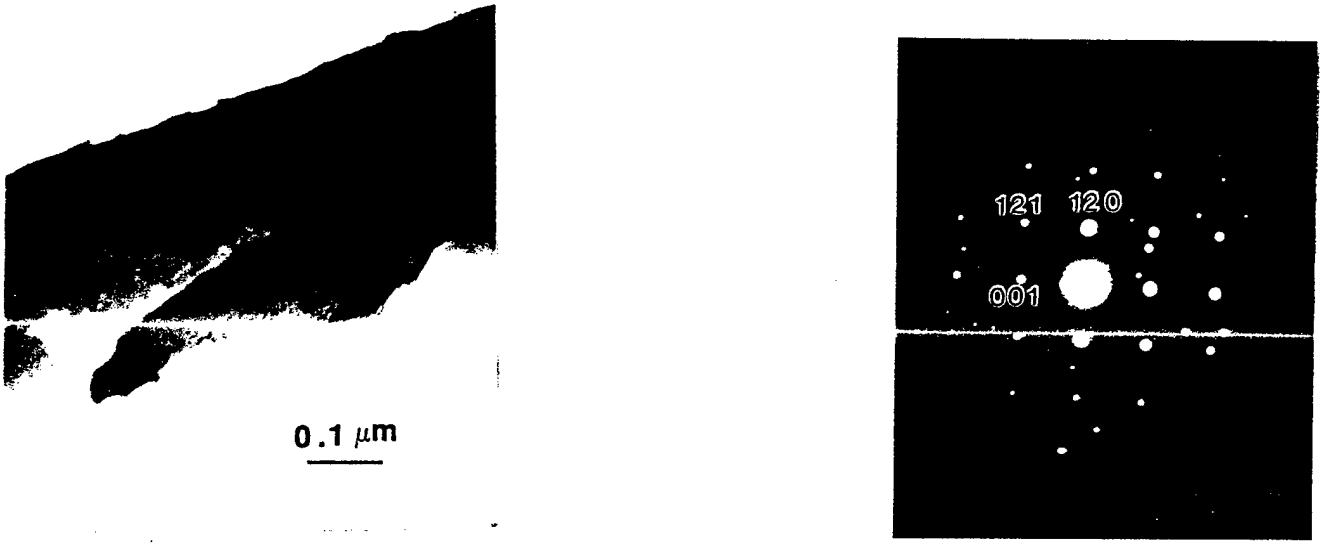

Figure 16. (a) Bright field TEM micrograph of individual mullite grain and (b) corresponding selected area diffraction pattern indexed as 3 $Al_2O_3 \cdot SiO_2$ mullite in the $[2\bar{1}0]$ zone axis.

3.5 Fiber Coating Research

Fiber coating research included (i) coating of fibers by the pulsed excimer laser ablation method, (ii) forming composite test materials with the coated fibers, and (iii) performing fiber push-out tests to evaluate the debonding shear strength, τ_d, of the coated fibers in the composite matrix material.

Preliminary experiments were performed, before the mullite fibers were available, to investigate the effects of enstatite ($MgSiO_3$) coatings on sapphire fibers and monazite coatings ($LaPO_4$) on YAG fibers. Later experiments were performed to deposit and characterize yttrium phosphate (YPO_4) coatings on the mullite fibers.

The YPO_4 and $LaPO_4$ coatings weaken the fiber-matrix bonding by an "interface-weakening" mechanism that toughens composite materials by allowing separation between the fiber and matrix to occur. Under a sufficient stress, separation occurs at the fiber-YPO_4 interface, which is weakened by the presence of oxygen atoms at the surfaces of both the fiber and the coating materials.

The enstatite coatings provide an "interphase-weakening" mechanism to toughen composite materials, in which failure under stress occurs within the bulk enstatite phase. The interphase-weakening is facilitated by a bulk phase transformation from a more dense phase at lower temperatures to a less dense phase at higher temperatures. A composite material

formed with the coated fibers is sintering or hot pressing at a temperature above that of the phase transformation. The fiber-matrix bonding is weakened when the composite is cooled below the transformation temperature to induce microcracks in the coating material that result from the volume contraction of the phase transition.

The debonding shear strength of fibers in composites that exhibit high performance, such as those formed by graphite-coated silicon carbide fibers in a silicon carbide matrix is on the order of 10-15 MPa. A goal in the present work was to investigate the interphase-weakening and interface-weakening mechanisms in composite materials for oxidizing environments by measuring τ_d values for coated oxide fiber composites and comparing the results with the typical values for the graphite-coated silicon carbide fiber composites.

3.5.1 Enstatite ($MgSiO_2$) Coatings on Sapphire Fibers

The interphase-weakening effect of enstatite ($MgSiO_3$) coatings on sapphire fibers was measured in an aluminum oxide matrix. The five layer coating scheme given in Figure 17 was used to prevent chemical reaction between enstatite and alumina at high temperature. The layers of aluminum titanate (Al_2TiO_5) and titanium dioxide (TiO_2) were used as chemical isolating layers between the aluminum oxide and enstatite.

Matrix: Alumina
5. Layer: Aluminum Titanate
4. Layer: Titania
3. Layer: Enstatite
2. Layer: Titania
1. Layer: Aluminum Titanate
Fibers: Sapphire

Figure 17. The coating arrangement for chemical bridging between enstatite and alumina fibers and matrix.

Aluminum titanate, titanium dioxide, and enstatite were produced as a target pellet of 2" diameter by 1/4" thick, for deposition by Pulsed Excimer Laser Ablation (PELA). The target pellets were sintered under the conditions given in Table VI.

Pulsed Excimer Laser Ablation (PELA) of the pellet materials onto silicon substrates was performed. SEM, XPS, and TEM studies of deposited layers were used to confirm that the

stoichiometry of the deposited layers was equal to that of the pellets. The pellet stoichiometry was independently confirmed by x-ray diffraction after sintering of the pellets.

Appropriate PELA deposition conditions were determined in experiments to deposit the coating materials on silicon substrates. The five layers were then deposited sequentially on the sapphire fibers. An SEM micrograph of a sapphire fiber and first three coating layers is shown in Figure 18.

Table VI. Sintering conditions for PELA target pellets

Material	Temperature	Sintering Time
Al_2TiO_5	1500°C	3 hr
TiO_2	1300°C	5 hr
$MgSiO_3$	1400°C	15 hr

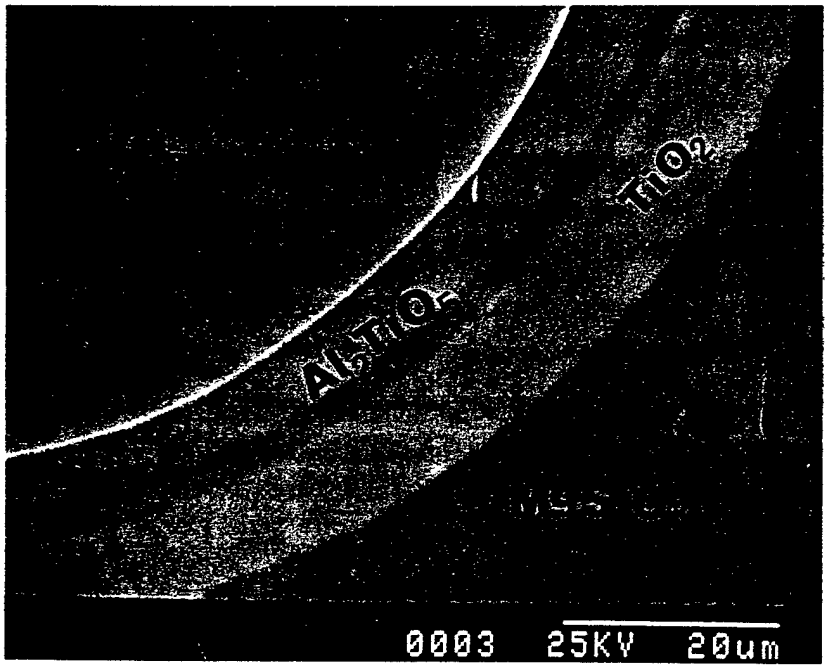

Figure 18. SEM micrograph of interfaces between sapphire fiber, aluminum titanate (Al_2TiO_5), titanium dioxide (TiO_2), and enstatite ($MgSiO_3$). (Cross sectional view).

3.5.2 Yttrium Phosphate (YPO_4) and Monazite ($LaPO_4$) Coatings

Yttrium phosphate, YPO_4, was selected as a coating material for the mullite fibers because of its chemical compatibility with mullite. Lanthanum phosphate (monazite) coatings were formed on YAG fibers and used to measure debonding shear strengths in an aluminum oxide matrix. The debonding sheer strength measurements were not possible on the coated mullite fibers because the fiber diameters were too small for use with the fiber push-out die. The monazite coatings on YAG fibers were formed by procedures similar to those described below for YPO_4 coatings on mullite fibers.

High purity yttrium phosphate was produced by the Pechini method. A disc-shaped pellet was formed and sintered at 1550°C for 3 hours. The pellet dimensions were 2.7 cm diameter by 0.7 cm thickness, to fit the laser ablation coating system chamber.

The mullite fibers were aligned in a special mount with a fiber spacing of 200-300 μm. The coatings were formed by Pulsed Excimer Laser Ablation (PELA), using a KrF excimer laser (LambdaPhysik, EMG201 MSC) with 248 nm wavelength, 270 mJ energy per pulse, and 10 Hz pulse repetition rate. The laser beam was focused to a spot size of 2.6 mm^2 on the YPO_4 disc-shaped target. The target was rotated at 16 rpm during the process and translated back and forth during the deposition process. The base pressure in the PELA system was approximately 3×10^{-7} Torr prior to deposition. Deposition of the coatings occurred under a continuous flow of oxygen gas at 0.1 Torr. Deposition time was 30 min for each side of the mullite fibers.

The coated fibers were used to form a composite test material (mullite matrix) by sintering at 1500°C for two hours. Figure 19 presents an SEM micrograph of the YPO_4-coated mullite fiber in the composite material. No decomposition of the fiber is evident, and a high chemical and dimensional stability is shown for the coated fiber in the composite at 1500°C.

Figure 19 reveals some porosity in the matrix and at the fiber-coating interface. The porosity may have resulted from different thermal expansion coefficients for the YPO_4 and mullite. Also, hot pressing is preferred to consolidate the composite, but was not used in this case. The bright region in the micrograph resulted from charging in an area where part of the composite was chipped away when the surface was polished. The coating thickness varies from about 2-5 μm on the 20 μm diameter fiber. The coating thickness could be made more uniform by some improvements in the PELA coating process. SEM/EDS verified the chemical composition of the coating and fiber materials.

3.5.3 Fiber Push-Out Tests

Table VII presents the results of fiber push-out tests on sapphire fibers coated with the five-layer enstatite coating and on YAG fibers coated with lanthanum phosphate. Both measurements are for fibers imbedded in an aluminum oxide matrix. It was not possible to perform push out tests on the coated mullite fiber composites because the die used for push-

out is 100 μm diameter and the fibers were of approximately 20 μm diameter. Typical data for graphite-coated silicon carbide fibers in a silicon carbide matrix are included in the table for comparison purposes.

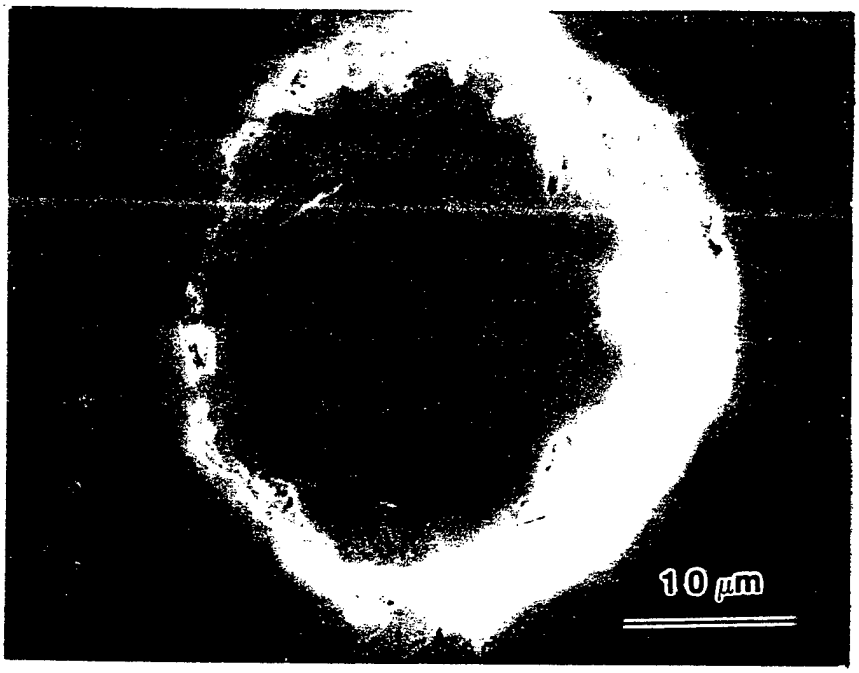

Figure 19. SEM micrograph of YPO_4-coated mullite fiber embedded in a mullite matrix and sintered at 1500°C for 2 hours. Heating and cooling rate: 5°C/min. The micrograph shows high chemical and dimensional stability of the coated mullite fiber composite at 1500°C.

Table VII. Debonding Shear Strength, t_d, from Fiber Push-Out Tests

Fiber, Coating, Matrix	Mechanism	τ_d, MPa
YAG fibers, $LaPO_4$ coating, Al_2O_3 matrix	Interface slippage	110
Sapphire fibers, 5-layer enstatite coating, Al_2O_3 matrix	Interphase weakening	ave: 25
Silicon carbide fibers, graphite coating, silicon carbide matrix	Interface slippage	10 - 15

It can be seen that the interphase weakening mechanism provides a debonding shear strength that approaches the values for graphite coated silicon carbide fibers in a silicon carbide matrix. Somewhat larger τ_d values are obtained for the phosphate coated fibers.

The composite with enstatite-coated sapphire fibers was initially formed by hot pressing at 1200°C, above the 865°C enstatite phase transformation temperature. Push out tests on the fibers resulted in fracture of the composite sample without any push out of the fiber. Fracture occurred at an applied shear stress of *ca.* 320 MPa. The absence of interphase weakening was attributed to the lack of a phase transformation on cooling in the as-prepared material, because the grain size was below the critical grain size for transformation. Grain growth during the subsequent annealing at 1350°C for 2 hours exceeded the critical particle size so that the transformation occurred spontaneously on cooling to room temperature. The accompanying anisotropic volume contraction weakened the mechanical connection between the fibers and the matrix, so that fiber push-out occurred at the low value of τ_d (25 MPa) reported in Table VII.

3.6 Process Scale-Up

Two methods to scale-up containerless melt processing for fiber synthesis were considered. The first is the conical nozzle levitation technique used in the current work. The second method, developed by Granier, *et al.* [25], employs gas-film levitation to make fluoride glass fibers by drawing the fibers from rather large masses of viscous metal fluoride melts. The containerless conditions yield fibers with exceptional purity and infrared transmission properties. The liquid levitation occurs in a shaped, porous container with levitation gas flow through the pores. Stable levitation occurs only for certain container shapes and porosities that depend on the liquid surface tension and density.

The gas-film levitation method is not recommended for the present application. We prefer the CNL approach, which (i) requires only a small amount of liquid to be maintained at high temperatures, reducing heating power costs, (ii) provides more stable access to the undercooled conditions, and (iii) uses an inexpensive levitation device that is not subject to failure.

Figure 20 illustrates the method by which the fiber drawing process may be scaled-up for production of continuous fibers at high drawing rates. It uses the conical nozzle levitator (CNL), which is a simple and inexpensive device to achieve the containerless conditions required to maintain undercooled liquids for fiber drawing. The levitation gas flow enters a plenum chamber and flows out through a larger nozzle where the liquid is levitated and also through a small orifice in the bottom of the plenum chamber through which fibers are drawn. Several fibers may be drawn simultaneously from a single levitated drop by use of a multiple stinger to initiate the fiber drawing. A large temperature gradient occurs in the liquid as a result of the intense laser heating at the top side and aerodynamic cooling at the bottom side of the levitated sample. The top of the liquid drop can thus be maintained above the melting

temperature, for continuous addition and melting of solid material to replenish that drawn away as fibers from the undercooled bottom side of the sample.

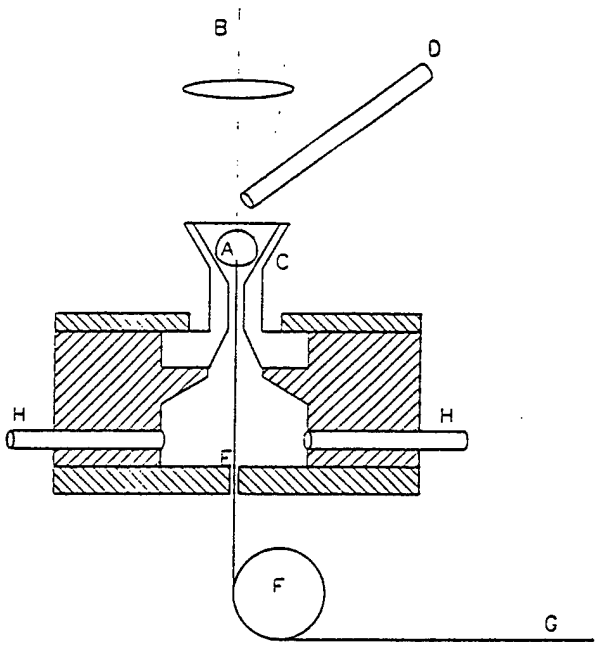

Figure 20. Method for producing continuous fibers by drawing from undercooled melt, using the conical nozzle levitator. A. Liquid drop that is superheated at the laser beam-heated top side and undercooled at the aerodynamically cooled bottom side; B, laser beam heating; C, aerodynamic levitation nozzle; D, tube to deliver powder for melting; E, orifice for fiber pulling; F, pulley; G, fiber; H, gas delivery to plenum chamber.

Laser heating requirements will be a major cost component of the fiber drawing process. A minimum laser energy requirement for mullite fiber drawing is that necessary to adiabatically heat and melt mullite, approximately 3.00 kJ/gram or 0.38 kW-hr/pound.

An estimate of the actual laser power requirement for the mullite fiber drawing process can be obtained from the following equation:

$$Q = Q_O / (\rho \, u \, \pi \, r^2 \, N) + \Delta H$$

In this equation, Q_O is the laser power required to maintain the molten drop, which is approximately 50 watts. ΔH is the energy per unit mass required to heat and melt the feed material, 3.0 kJ/gram. The fiber production rate (mass per unit time) is give by the product of density (ρ), fiber pulling velocity (u), fiber cross sectional area ($\pi \, r^2$), and the number (N)

of fibers that are simultaneously pulled from the liquid drop. The density of mullite is ρ = 3.16 g/cm^3. Using fiber drawing conditions based on the results of this research, with r = 12.5 μm, u = 100 cm/s, and N = 9, we obtain Q = 6.58 kJ/kg, or 0.83 kW-hr/pound. The fiber drawing rate would be 50 grams/hour and the laser power requirement would be increased to approximately 92 watts to provide the heating and melting energy.

Beam splitters can be used to separate the beam of our 500 watt CO_2 laser into 4 beams of *ca.* 100 watts each, after subtracting estimated laser power transmission losses, to operate four fiber drawing stations in which 9 fibers may be drawn at each station. This arrangement would provide a tow of 36 fibers at a mass production rate of up to 10 lb per 24-hour day. The development of this continuous fiber drawing capability will be a key task in the proposed Phase II SBIR research.

3.6.1 Economics of Scale-up

Table VIII presents our analysis of fiber production costs for facilities with three different production capacities, of about 2,660, 26,600 and 266,000 lb/year of mullite fibers. The table is divided into four parts showing the process assumptions for fiber growth stations, estimated capital investment requirements, calculated fiber production rates, and the operating costs.

The estimated fiber production costs decrease considerably with production rate, from over $300 per pound for the small scale production unit to about $40 per pound for the large scale unit. Significant economies of scale have been assumed in the capital investment required to build the facilities, but the most important economy of scale would be in the cost of labor. The actual cost of small scale production (about 2,660 pounds/year) would be expected to exceed that given in Table VIII because small scale production for the assumed 5-year operating period would be unlikely. A more realistic estimate of costs for the small scale production unit might assume a one-year life.

In conclusion, we find that it should be possible to manufacture mullite fibers on a relatively large scale at operating costs significantly under $100 per pound. Smaller-scale production can be developed at a total cost of about $1,000,000 to supply fibers in quantities sufficient for composite materials development projects. The manufacturing method has application to a variety of other oxide fiber materials, *e.g.*, YAG fibers, and further research would be required to estimate the costs for these fibers. However, it is not expected that major differences in cost would result.

3.7 Market Research

We are reviewing the literature and talking to applications experts from industry, national laboratories, and academia. The consistent message is that there is a critical need for improved, more cost-effective high-temperature reinforcing fibers in a variety of industrial areas. In a recent survey of over 120 R&D and industrial organizations, the need for

Table VIII. Analysis of Fiber Production Costs

I. PROCESS ASSUMPTIONS (SINGLE FIBER GROWTH STATION)

Fiber material	mullite	
Fiber density	3.16	g/cm3
Fibers per growth station	9	
Fiber diameter, d	25	micrometers
Fiber pulling rate, u	100	cm/s
On-stream time	250	days/year
Fiber production rate	302	kg/year
Fiber pulling temperature	1,400	C
Ambient temperature	25	C
Yield	90	%
Laser power per fiber growth station	100	watts
Laser electrical efficiency	5	%
Laser power transmission losses	20	%
Total laser power	125	watts
Laser electrical power	2.50	Kw

II. CAPITAL INVESTMENT*

Number of fiber growth stations, N	4	40	400
Fiber growth systems	$16,000	$80,190	$401,902
CO2 lasers	90,000	451,069	2,260,698
Optics	4,500	22,553	113,035
Fiber pulling systems	2,500	12,530	62,797
Gas handling systems	5,000	25,059	125,594
Safety	10,000	50,119	251,189
Product packaging	5,000	25,059	125,594
Subtotal	$133,000	$666,579	$3,340,809
Installation costs, 30%	39,900	199,974	1,002,243
Subtotal	$172,900	$866,553	$4,343,052
One-time development costs	300,000		
Engineering, 30%	51,870	259,966	1,302,915
Contingency, 30%	51,870	259,966	1,302,915
Total capital investment	$576,640	$1,386,484	$6,948,883
Capital investment per pound of fibers/year	$1,053.02	$253.19	$126.90

* Capital investment for N systems proportional to N**0.7

Table VIII (Continued). Analysis of Fiber Production Costs

III. FIBER PRODUCTION RATES			
Number of growth stations	4	40	400
Fiber production rate, kg/yr	1,206	12,062	120,618
Fiber production rate, lb/yr	2,657	26,568	265,679
IV. OPERATING COSTS			
Number of growth stations	4	40	400
Operating labor per shift	2	4	16
Total laser power required	500	5,000	50,000
Mullite feedstock, initially $20/pound**	$34,164	$215,560	$1,360,094
Laser power, $0.1/Kw-hr	6,000	60,000	600,000
Labor***	328,652	731,263	3,462,452
Supervisions and overheads****	295,786	658,137	3,116,207
Maintenance supplies, 10% of capital	57,664	138,648	694,888
Depreciation, straight line, 5 yr	115,328	277,297	1,389,777
Total operating costs	$837,594	$2,080,906	$10,623,418
Operating cost per kg of fibers	$694	$173	$88
Operating cost per pound of fibers	$315	$78	$40

** Feedstock costs proportion to quantity**0.8

*** Includes operating labor &quality control labor of 0.04 person per fiber reactor system at $18/hr plus 30% fringe benefits, plus maintenance labor at 5% of capital investment.

**** Supervision & overheads at 90% of operating, quality control, and maintenance labor.

improved reinforcing fibers was rated the top priority [13]. Promising applications include high-temperature turbine engine components, exhaust nozzles, thrust deflectors, combustor liners in power generators, radiant burners, heat shields, and high-temperature gas filters.

The key issues for reinforcing fibers are: (i) performance: (*e.g.*, room temperature properties such as strength and elastic modulus and high temperature properties such as creep, rupture stress, and oxidation resistance); (ii) production capacity; and (iii) cost. The key properties and the order of importance of these issues depends on the application. There is a strong need for fibers capable of performing at temperatures above at least 1200°C (preferably above 1350°C). Some lower-volume applications can support fibers costing up to $200/pound or more. Larger volume applications will begin to open up if fibers can be supplied for less than $100 per pound.

During Phase II, we will estimate demand *versus* price curves for fibers with various properties. We will then use these curves and our estimated costs to select initial target markets. We would likely choose small volume/high price applications first, then develop a larger-scale fiber production facility to reduce product costs and access the higher volume markets.

4. TECHNICAL FEASIBILITY

The technical feasibility of making strong oxide fibers was demonstrated by the present work. The experiments using a conical nozzle levitator showed a technically viable and cost effective method to scale-up production of oxide fiber materials. The feasibility of using interphase-weakening coatings on oxide fibers to achieve toughness in composite materials for oxidizing conditions was also demonstrated.

We are developing agreements under which we will team up with potential clients and fiber users during the Phase II research. Once the performance is established in the research environment, we expect that the fibers will compete with other oxide fibers in performance/price. Commercial markets will be developed during the Phase II SBIR research and in the early stages of the Phase III.

We have developed a detailed plan for scaled-up production of fibers which will be presented in the Phase II proposal and executed during the Phase II research.

5. REFERENCES

1. J.K.R. Weber, S. Krishnan and P.C. Nordine, "The Use of Containerless Processing in Researching Reactive Materials," J. Metals, **43**, 8 (1991).

2. J.K.R. Weber, D.R. Merkley, C.D. Anderson, P.C. Nordine, C.S. Ray and D.E. Day, "Enhancement of Calcia-Gallia Glass Formation by Containerless Processing," J. Am. Ceram. Soc., **76**, 2139 (1993).

3. J.K.R. Weber, W.P. Zima, P.C. Nordine, K.C. Goretta, and R.B. Poeppel, "Containerless Processing of Ceramic Superconductors," Containerless Processing Techniques and Applications, Eds. W.H Hofmeister and R.A. Schiffman, TMS, Warrendale, PA, pp 123-28 (1993).

4. J.R. Olive, W.H. Hofmeister, R.J. Bayuzick, G. Carro, J.P. McHugh, R.H. Hopkins, M. Vlasse, J.K.R. Weber, P.C. Nordine and M. McElfresh, "Formation of Tetragonal $YBa_2Cu_3O_{7-\delta}$ from an Undercooled Melt", J. Mat. Res., **9**, 1 (1994).

5. J.K.R. Weber, D.S. Hampton, D.R. Merkley, C.A. Rey, M.M. Zatarski and P.C. Nordine, "Aero-acoustic Levitation - A method for containerless liquid phase processing at high temperatures," Rev. Sci. Instrum., **65**, 456-465 (1994).

6. J.K.R. Weber, C.D. Anderson, S. Krishnan and P.C. Nordine, "Structure of Aluminum Oxide Formed from Undercooled Melts," J. Am. Ceram. Soc., **78**, 577-82 (1995).

7. J.K.R. Weber, P.C. Nordine, K.C. Goretta, and R.B. Poeppel, "Effects of oxygen pressure on the structure of Y-Ba-Cu-O Materials formed by Containerless Melting and Solidification," J. Mat. Res. **9**, 1657 (1994).

8. J.K.R. Weber, S. Krishnan, C.D. Anderson and P.C. Nordine, "Spectral Absorption Coefficient of Liquid Aluminum Oxide from 0.420-0.780 μm," J. Am. Ceram. Soc., **78**, 583-87 (1995).

9. A.B. Biswas, J.K.R. Weber and P.C. Nordine, "Cr^{3+} Fluorescence in Containerless Melt-purified Aluminum Oxide" J. Mat. Res. **10**, 1823-27 (1995).

10. J.K.R. Weber, "Containerless Property Measurements on Molten Aluminum Oxide and Alumino-Silicate Binary Mixtures," Proc. 4th Asian Thermophysical Properties Conference, Tokyo, 5-8 Sept., 1995, Ed. A. Nagashima, pp. 873-876.

11. C.M. Huang. F. Xiong, Y.Xu, A. Zangvil and W.M. Kriven, "Laser Ablation Coatings on Ceramic Fibers for Ceramic Matrix Composites," J. Materials Sci. Eng., in press.

12. W.M. Kriven, "Displacive Transformations and their Applications in Structural Ceramics," J. De Physique IV, **5**, C8, 101-110 (1995).

13. R.A. Lowden and M.A. Karnitz, "A survey of the Status of Ceramic Reinforcement Technology and its Relationship to CFCCs for Industrial Applications," Oak Ridge National Laboratory, Oak Ridge, TN (1996).

14. K.C. Chen, K.S. Mazdiyasni, and H.H. Streckert, "Ceramic Fiber Feasibility Studies," Materials Directorate, Wright Laboratory, Air Force Materiel Command, Wright Patterson AFB OH Report WL-TR-94-4022, July 1993.

15. J.M. Collins, H.E. Bates, and J.J. Fitzgibbon, "Growth and Characterization of Single Crystal YAG Fibers," Materials Directorate, Wright Laboratory, Air Force Materiel Command, Wright Patterson AFB OH Report WL-TR-94-4085, June 1994.

16. J.W. Halloran, R.M. Laine, B.H. King, and Y. Liu, "Creep Resistant Oxide Fibers," Materials Directorate, Wright Laboratory, Air Force Materiel Command, Wright Patterson AFB OH Report WL-TR-94-4100, March 1994.

17. T.L. Tompkins, "Ceramic Oxide Fibers: Building Blocks for New Applications," Ceramic Industry, April 1995

18. G. Urbain, "Viscosity of Liquid Alumina," Rev. Int. hautes Temper. Refract. **19**, 55 (1982).

19. G. Urbain, "Viscosity and Structure of Aluminosilicate Melts," Rev. Int. hautes Temper. Refract. **11**, 133 (1974).

20. I.A. Aksay and J.A. Pask, "Stable and Metastable Equilibria in the System SiO_2-Al_2O_3," J. Am. Ceram. Soc., **58**, 507 (1975).

21. J.K.R. Weber, J.J. Felten and P.C. Nordine, "New Method for High Purity Ceramic Synthesis," Rev. Sci. Instrum., , (1996).

22. M. Mizuno and H. Saito, "Preparation of Highly Pure Fine Mullite Powder," J. Am. Ceram. Soc. **72**, 377-82 (1989).

23. J.K.R. Weber and P.C. Nordine, "Containerless Liquid-Phase Processing at High temperatures," Microgravity Science and Technology, VII, 279-282 (1995).

24. J.K.R. Weber and P.C. Nordine, unpublished.

25. J. Granier and C. Potard, "Elaboration et Moulage sans Conteneur par la Methode des Films de Gaz: Demonstration et Modelixation Preliminaires," in Proc. 6th European Symp. on Mat. Sci. under microgravity conditions, ESA SP-256 (1987), pp. 421-425.

26. C.M. Huang, Y. Xu, F. Xiaong, A. Zangvil and W.M. Kriven, "Laser Ablation Coatings on Ceramic Fibers for Ceramic Matrix Composites," J. Mat. Sci. and Eng., **A191**, 249-56 (1995).

27. A. Sayir and L.E. Matson, "Growth and Characterization of Directionally Solidified $Al_2O_3/Y_3Al_5O_{12}$ (YAG) Eutectic Fibers," NASA Conf. Publications 10082 (199a) pp. 83-1-83-13.

28. C.M. Huang, D.H. Kuo, Y.J. Kim and W.M. Kriven, "Phase Stability of Chemically Derived Enstatite ($MgSiO_2$) Powders," J. Am. Ceram. Soc. **77**, 2625 (1994).